EMBO reports

TRANSPARENT PROCESS

scientific report

Autophagy modulates miRNA-mediated gene silencing and selectively degrades AIN-1/GW182 in *C. elegans*

Peipei Zhang[1,2,3] *& Hong Zhang*[3+]

[1]College of Life Sciences, Beijing Normal University, Beijing, [2]National Institute of Biological Sciences, Beijing, and [3]State Key Laboratory of Biomacromolecules, Institute of Biophysics, Chinese Academy of Sciences, Beijing, PR China

MicroRNAs (miRNAs) post-transcriptionally repress gene expression via the miRNA-induced silencing complex (miRISC), which includes miRNA, Argonaute and a GW182 family member. Here we show that in *Caenorhabditis elegans*, miRNA-mediated gene silencing is modulated by macroautophagy, a lysosome-mediated degradation process. Loss of autophagy activity suppresses developmental defects caused by partially impaired silencing of miRNA targets including the *let-7* family and *lsy-6*. The *C. elegans* GW182 homolog AIN-1 is itself selectively degraded by autophagy and colocalizes with the p62 homolog SQST-1 in autophagy mutants. Thus, autophagy activity modulates miRNA-mediated gene silencing and degrades a core miRISC component.

Keywords: Argonaute; autophagy; *C. elegans*; GW182; miRNA

EMBO *reports* (2013) **14,** 568–576. doi:10.1038/embor.2013.53

INTRODUCTION

MicroRNAs (miRNAs), a class of evolutionarily conserved ~22 nucleotide RNAs, post-transcriptionally repress gene expression through non-perfect base pairing to the 3′ untranslated region (UTR) of target mRNAs, affecting translational efficiency and/or stability [1]. The repressive effect of miRNAs is mediated by the miRNA-induced silencing complex (miRISC), which includes miRNA, Argonaute (AGO) and a GW182 family member [2]. miRNA-mediated gene silencing regulates a variety of developmental and cellular processes. In *Caenorhabditis elegans*, miRNAs control developmental timing of diverse post-embryonic cell lineages by regulating stage-specific expression of a group of heterochronic genes [3]. For example, the *let-7* family miRNAs (*mir-48*, *mir-84* and *mir-241*) repress the Hunchback homolog *hbl-1* to control succession from the L2 to L3 larval stage, while *let-7* miRNA downregulates the expression of *lin-41* in specifying the L4-adult switch [4–6]. Loss of function of the miRNA pathway results in retarded heterochronic defects, in which the stage-specific fate is reiterated and terminal differentiation is delayed [3]. The *let-7* family miRNAs also negatively regulates *let-60/RAS*, a key component in vulval cell fate specification [7]. Loss of *let-60/RAS* activity causes a vulvaless phenotype, while gain of function of *let-60* activity results in generation of supernumerary vulva-like structures, a phenotype known as multivulva (Muv) [8]. The *lsy-6* miRNA controls left–right asymmetry of the two taste receptor neurons, ASE left (ASEL) and ASE right (ASER) [9]. *lsy-6*, which is expressed in ASEL, but not in ASER, exerts its effect by repressing the Nkx-type homeobox gene *cog-1* [9]. miRNA-mediated silencing of target genes in these developmental processes has been shown to be modulated by various factors, including the TRIM-NHL family protein NHL-2 and Wnt signaling [10,11].

Autophagy is an evolutionarily conserved intracellular degradation process, involving the formation of a closed double-membrane compartment called the autophagosome, and its subsequent delivery of sequestrated materials to the lysosome for degradation [12]. Several *Atg* (autophagy-related) and *epg* (ectopic PGL granules) genes have been identified that act at discrete steps of autophagosome formation in higher eukaryotes [12–14]. For example, the serine/threonine kinase Atg1/Atg13 complex and the class III phosphatidylinositol 3-kinase, Vps34/Atg6 complex are required for initiation and nucleation of the isolation membrane. The two ubiquitin-like systems, consisting of Atg8(ubiquitin-like molecule)/Atg7(E1-like activating enzyme)/Atg3(E2-like conjugating enzyme) and Atg12(ubiquitin-like molecule)/Atg7/Atg10(E2-like enzyme), are essential for the expansion and closure of the isolation membrane to form the autophagosome. The Atg2/Atg18 complex is involved in cycling of the transmembrane protein Atg9, which supplies membranes for the formation of autophagosomes [12]. EPG-5 is involved in the autophagosome maturation [13,15]. Basal autophagy selectively removes aggregate-prone proteins or damaged organelles, functioning as a quality control system. A family of Atg8/LC3(mammalian Atg8 homolog) interacting

[1]College of Life Sciences, Beijing Normal University, Beijing 100875
[2]National Institute of Biological Sciences, Beijing 102206
[3]State Key Laboratory of Biomacromolecules, Institute of Biophysics, Chinese Academy of Sciences, Beijing 100101, PR China
[+]Corresponding author. Tel: +86 10 64848238; Fax: +86 10 64853925; E-mail: hongzhang@sun5.ibp.ac.cn

Received 30 November 2012; revised 8 April 2013; accepted 9 April 2013; published online 26 April 2013

proteins act as receptors that mediate delivery of specific cargoes to the autophagic machinery through Atg8 binding [16]. Selective removal of RNA-induced silencing complex (RISC) components by autophagy has recently emerged as a mechanism for modulating small interefering RNA (siRNA) or miRNA activity. In *Arabidopsis*, the viral suppressor of RNA silencing protein P0, which is a component of an E3 ligase, triggers the degradation of ARGONAUTE1 by autophagy [17]. In mammalian cells, DICER and AGO2 are targeted for selective autophagic degradation by the receptor NDP52 [18].

Here we show that during *C. elegans* development, autophagy modulates miRNA-mediated cell fate specification and selectively removes AIN-1, a key component of miRISC. Our study reveals a role of autophagy in cell-fate specification by modulating miRNA-mediated gene silencing.

RESULTS AND DISCUSSION

Role of autophagy in the heterochronic pathway

miRNAs play an important role in controlling the developmental timing of a row of lateral hypodermal seam cells, which undergo stage-specific developmental programs and increase in number from 10 at hatching to 16 from the L2 larval stage onwards (Fig 1A–C). At the late L4 larval stage, seam cells terminally differentiate, resulting in synthesis of adult-specific cuticular structures called alae (Fig 1D). Mutants of autophagy genes acting at distinct steps of autophagosome formation, including *lgg-1/Atg8*, *atg-3*, *epg-8/Atg6*, *epg-6* and *atg-2*, exhibited normal seam cell development (Fig 1E,F; Table I).

We tested whether loss of autophagy activity modulates phenotypes associated with loss-of-function mutants of miRISC components. Reduced activity of *dcr-1* (the single *C. elegans* Dicer homolog), *alg-1* (one of two Ago homologs) and *ain-1* (ALG-1 interacting protein 1, one of two GW182 homologs) impairs miRNA-mediated downregulation of two heterochronic genes, *hbl-1* and *lin-41*, and causes reiteration of the L2-specific seam cell proliferation programs at the L3 larval stage and delayed terminal differentiation [19–21]. *dcr-1(bp132)* contains an aspartate-to-asparagine mutation in the RNase III domain and causes reduced levels of mature miRNAs [11]. *dcr-1*(*bp132)* young adults have an average of 28.9 seam cells compared to 16.0 in wild type and 81.1% of mutants exhibited incomplete terminal differentiation of seam cells with gaps in the alae (Fig 1G,H). Loss of function of *atg-2* suppressed the retarded heterochronic defect in *dcr-1*(*bp132)* mutants. In *dcr-1*; *atg-2* double mutants, the average number of seam cells was 20.2, and 41.7% of *dcr-1; atg-2* double mutants showed completely fused alae structures (Figs 1I,J; Table I). Loss of activity of autophagy genes, including *epg-1*, *atg-7*, *epg-6* and *epg-5*, also partially suppressed the retarded heterochronic defect in *ain-1* or *alg-1* loss-of-function mutants (Table I). Suppression of the heterochronic defect in *ain-1* and *alg-1* mutants by loss of autophagy activity suggests that additional targets might function to modulate miRNA activity.

We further examined whether autophagy interacts with other heterochronic mutants. The zinc-finger gene *sea-2* regulates expression of the heterochronic gene *lin-28* at the post-transcriptional level [22]. Mutations in *sea-2* cause retarded heterochronic defects. We found that *atg-2* mutants suppressed the retarded terminal differentiation defect in *sea-2* mutants (Table I). In contrast, loss of activity of autophagy genes, including *epg-6* and *atg-2*, enhanced the precocious heterochronic defect associated with *lin-41* hypomorphic mutants (Table I).

To determine whether autophagy regulates miRNA-mediated silencing of downstream targets, we examined the expression of reporters for *hbl-1* and *lin-41*, two genetically verified targets of *let-7* miRNAs. Expression of a *hbl-1::gfp::hbl-1* reporter is strong in the ventral nerve cord (VNC) at larval stages before early L4, then greatly diminishes in late L4 and adult animals [23,24]. Downregulation of HBL-1::GFP in VNC is mediated by *let-7* and also *lin-4* miRNAs [23,24]. The fluorescence intensity of HBL-1::GFP in VNC was significantly reduced in *atg-2* and *epg-6* autophagy mutants (Fig 1K–N). We further examined the expression of a hypodermally expressed reporter, *col-10::gfp::lin-41 (3′ UTR)*, which contains the *lin-41 3′ UTR*. The *let-7* binding sites present in the *lin-41 3′ UTR* sufficiently mediate the downregulation of *lin-41* by *let-7* [4]. Expression of this reporter is strong at larval stages, but decreases from the late L4 stage onwards [25]. In autophagy mutants, the same transgene was much more weakly expressed in late L4 animals (Fig 1O–R). Activating autophagy by inactivation of Tor signaling or starvation increased the expression of *hbl-1::gfp::hbl-1* in VNC and *col-10::gfp::lin-41 (3′ UTR)* in hypodermal cells (Fig 1S,T). The elevated expression of these reporters in *let-7* mutants was not affected by loss of autophagy activity (supplementary Figs S1A–H online). These results indicate that loss of autophagy activity enhances *let-7*-mediated downregulation of target genes.

Autophagy mutants suppress the *let-60(gf)* Muv defect

We determined if autophagy activity regulates expression of another *let-7* family miRNA target, *let-60/RAS* [7], which is essential for vulval cell fate specification. The vulval precursor cell fate is sensitive to the dosage of *let-60* activity [8]. *let-60(n1046gf)*, a gain-of-function mutation, results in elevated LET-60 activity and a Muv phenotype (Figs 2A,B). Autophagy mutants did not show defects in vulval development, but simultaneous loss of autophagy gene activity in *let-60(n1046gf)* mutants, including *epg-6, atg-2* and *epg-5,* dramatically reduced the Muv phenotype (Figs 2C,D). The suppression effect was partially reduced by loss of *ain-1* activity (Fig 2D). *mpk-1*, encoding a mitogen-activated protein kinase, acts downstream of *let-60* in controlling vulval development [8]. Hyperactive *mpk-1* mutants, *gaIs37*, exhibited a Muv phenotype in 98.8% of animals ($n = 322$) at 24 °C. The Muv phenotype in *gaIs37* mutants was not affected by loss of *epg-5* activity (98.3% Muv, $n = 294$).

Loss of autophagy activity suppresses *lsy-6(hypo)*

The non-*let-7*-family miRNA *lsy-6* specifies the fates of two neurons, ASEL and ASER, by downregulating *cog-1* in ASEL [9]. Loss of *lsy-6* activity causes the ASEL neuron to adopt the ASER fate (Figs 2E,F) [9]. Transformation of ASEL to ASER was complete in *lsy-6(ot71)* null animals but incomplete in animals bearing a hypomorphic allele of *lsy-6(ot150)* (Fig 2G). Loss of function of autophagy genes did not cause defects in ASEL fate specification, visualized by the ASEL-specific reporter *lim-6^{pro}::GFP* (Fig 2G). Autophagy mutants, including *epg-1*, *atg-2*, *atg-7*, *epg-6* and *epg-5*, partially rescued the ASEL fate specification phenotype in *lsy-6(ot150)* mutants (Fig 2G). Elevated autophagy activity, caused by TOR signaling mutations including *let-363/Tor* and *rheb-1*, exacerbated the ASEL specification defect in *lsy-6(ot150)* mutants

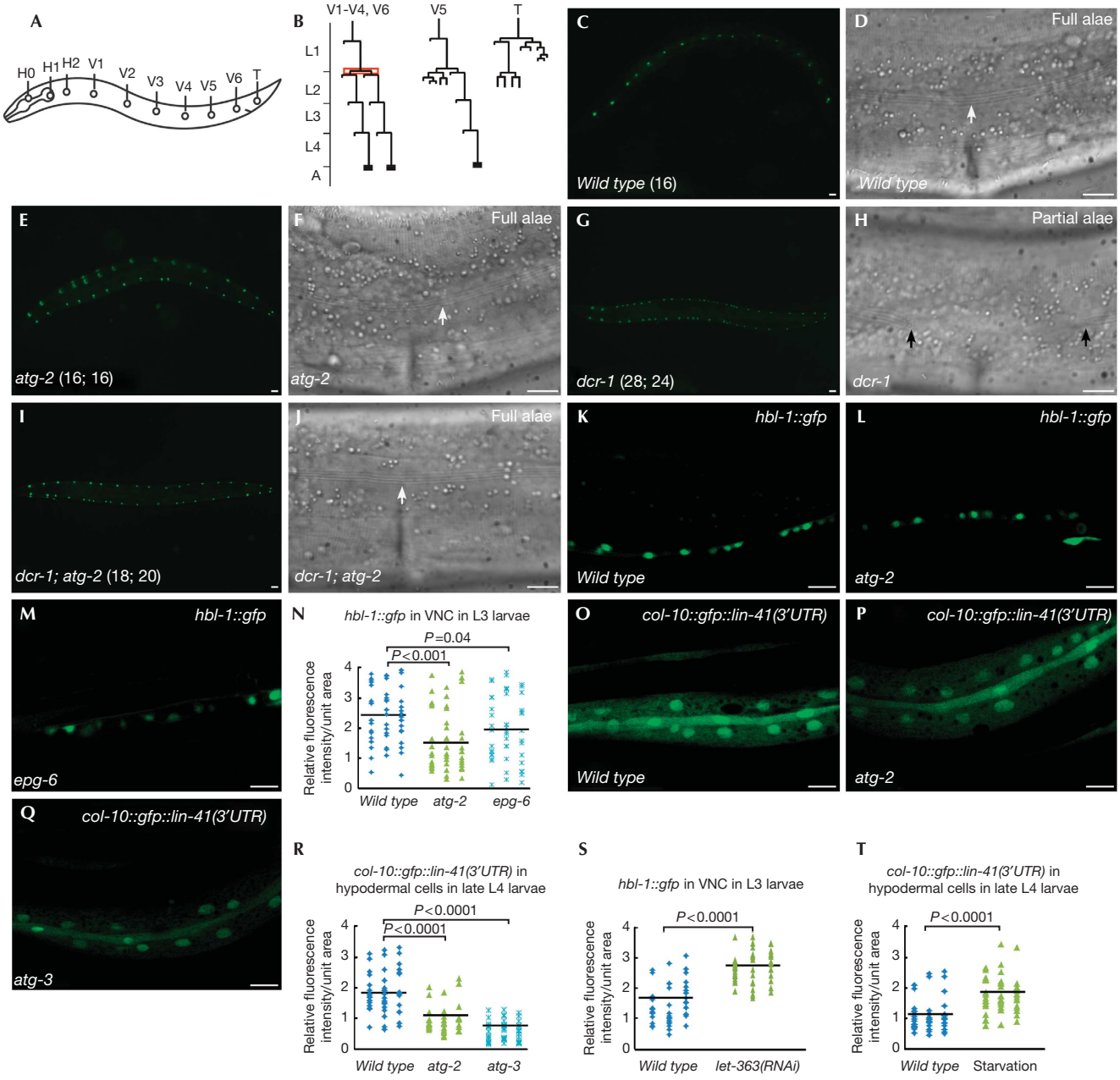

Fig 1 | Loss of autophagy activity suppresses the retarded heterochronic defects in miRISC mutants. (**A**) Schematic illustration of seam cells in a wild-type L1 larva. (**B**) Division pattern of seam cells at the postembryonic stage in hermaphrodites. Seam cells V1–V4 and V6 divide symmetrically at the L2 stage (highlighted in red), thus doubling in number. (**C–F**) At the young adult stage, wild-type and *atg-2* mutant animals have 16 seam cells on each side, visualized by the seam cell-specific marker *scm::gfp*. Cuticular alae (arrow) run continuously from anterior to posterior. The number of seam cells is shown in brackets. (**G,H**) *dcr-1* young adults have an increased number of seam cells (shown in brackets) and gaps in the alae (between arrows). (**I,J**) *atg-2* mutations suppress the retarded heterochronic defect in *dcr-1* mutants. Complete alae (arrow) are formed in *dcr-1; atg-2* double mutants. (**K–M**) Confocal images showing expression of *hbl-1::gfp::hbl-1* reporter in VNC in wild type (**K**), *atg-2* (**L**) and *epg-6* (**M**) L3 larvae. (**N**) Distribution of relative fluorescence intensity of HBL-1::GFP in 50 unit areas in VNC in the indicated strains. (**O–Q**) Confocal images showing the expression of the *col-10::gfp::lin-41(3′UTR)* reporter in wild type (**O**), *atg-2* (**P**) and *atg-3* (**Q**) late L4 larvae. (**R**) Distribution of relative fluorescence intensity of *col-10::gfp::lin-41(3′UTR)* in 50 unit areas of hypodermal cells in the indicated strains. (**S,T**) Distribution of relative fluorescence intensity of *hbl-1::gfp* in VNC and *col-10::gfp::lin-41(3′UTR)* in hypodermal cells in 50 unit areas in wild type, *let-363(RNAi)* or starvation-treated animals. Black lines in (**N,R–T**) represent the average fluorescence intensity of the reporter in each strain. *P* values are determined by Student's two-tailed unpaired *t*-test in (**N,R–T**). (**C,E,G,I**) Scale bar, 20 μm; (**D,F,H,J–M,O–Q**) scale bar, 10 μm. GFP, green fluorescent protein; miRISC, miRNA-induced silencing complex; RNAi, RNA-mediated interference; UTR, untranslated region; VNC, ventral nerve cord.

Table I|Genetic interaction between autophagy and heterochronic mutants

Genotype	Number of seam cells (n)	*P* value	Percentage of animals with alae formation (%)					*n*	*P* value
			L3 molt		L4 molt				
			No	Partial	Full	Partial	No		
Wild type	16.0 (26)		0	0	100	0	0	26	
epg-6	16.0 (25)	0.70	0	0	100	0	0	22	
atg-7	16.0 (33)	1.00	0	0	100	0	0	19	
atg-2	16.0 (30)	0.80	0	0	100	0	0	21	
epg-1	15.8 (34)	0.12	0	0	100	0	0	20	
epg-5	15.9 (32)	0.88	0	0	100	0	0	18	
dcr-1(bp132)	28.9 (33)		ND	ND	13.5	81.1	5.4	37	
dcr-1(bp132); atg-2	20.2 (40)	<0.001	ND	ND	41.7	52.8	5.5	36	0.004
dcr-1(bp132); atg-7	25.3 (46)	0.001	ND	ND	18.9	76.7	5.4	37	0.81
ain-1(bp299)	21.0 (25)		ND	ND	24.3	75.7	0	37	
epg-6; ain-1(bp299)	19.1 (25)	<0.001	ND	ND	67.8	32.2	0	43	<0.001
epg-5; ain-1(bp299)	17.9 (29)	<0.001	ND	ND	70.0	30.0	0	28	<0.001
ain-1(ku322)	21.5 (46)		ND	ND	52.2	47.8	0	33	
epg-6; ain-1(ku322)	19.2 (58)	0.002	ND	ND	92.9	7.1	0	28	0.02
epg-1; ain-1(ku322)	18.8 (33)	0.01	ND	ND	86.7	13.3	0	30	0.008
epg-5; ain-1(ku322)	18.0 (46)	0.002	ND	ND	86.2	13.8	0	29	0.009
atg-7; ain-1(ku322)	19.1 (44)	0.02	ND	ND	82.1	17.9	0	28	0.02
alg-1(gk214)	ND		ND	ND	0	53.1	46.9	32	
epg-6; alg-1(gk214)	ND		ND	ND	8.0	68.0	24.0	28	<0.001
atg-7; alg-1(gk214)	ND		ND	ND	38.9	61.1	0	18	<0.001
sea-2(bp283)	19.5 (38)		ND	ND	63.6	36.4	0	22	
sea-2(bp283); epg-6	19.5 (36)	0.97	ND	ND	83.3	16.7	0	18	0.16
sea-2(bp283); atg-2	16.8 (34)	<0.001	ND	ND	89.2	10.8	0	28	0.04
lin-41(ma104)	ND		91.4	8.6	ND	ND	ND	35	
lin-41(ma104); epg-6	ND		71.9	28.1	ND	ND	ND	32	0.04
lin-41(ma104); atg-2	ND		45.0	55.0	ND	ND	ND	20	0.002

Abbreviations: full, complete alae; n, number of animal sides examined; ND, not determined; no, no alae; partial, gaps in alae. Animals containing *sea-2(bp283)* were grown at 15 °C. *P*-values are determined by student's two-tailed unpaired *t*-test.

(Fig 2G). Loss of autophagy activity did not suppress the defect in *lsy-6(ot71)* null animals (Fig 2G), indicating that autophagy mutants could not bypass the requirement of *lsy-6* activity for specification of ASEL fate. In summary, loss of autophagy activity suppresses developmental defects associated with impaired gene silencing mediated by diverse miRNAs.

AIN-1/GW182 is selectively removed by autophagy

We next examined the expression of *C. elegans* miRISC components, including the GW182 homologs AIN-1 and AIN-2, and the Ago homologs ALG-1 and ALG-2.*ain-1* and *ain-2* or *alg-1* and *alg-2* function redundantly. *ain-1* and *alg-1* single mutants show retarded heterochronic defects, while *ain-2* and *alg-2* single mutants have no evident defects. *ain-1/-2* or *alg-1/-2* double mutants display much stronger defects than either single mutant [19–21]. In wild-type embryos, AIN-1::GFP was diffusely expressed in the cytoplasm during embryogenesis (Figs 3A,B). In autophagy mutants, including *epg-6, atg-3, epg-8* and *atg-2,* AIN-1::GFP was strongly expressed and accumulated into a large number of aggregates (Figs 3C,G; supplementary Figs S2A,B online). Levels of endogenous AIN-1 protein, but not *ain-1* mRNA, were increased in autophagy mutants (Fig 3D; supplementary Figs S2C,D online). These results indicate that AIN-1 is degraded by autophagy. Expression of AIN-2::GFP, which is diffusely localized in wild-type embryos, was unaffected in autophagy mutant embryos (supplementary Figs S2E,F online).

Translational fusion reporters for *gfp::alg-1* and *alg-2::gfp* were both diffusely expressed in the cytoplasm of most embryonic cells (Figs 3I,J; supplementary Figs S2I,J online). A few ALG-1 and ALG-2 aggregates were formed in autophagy mutants but the

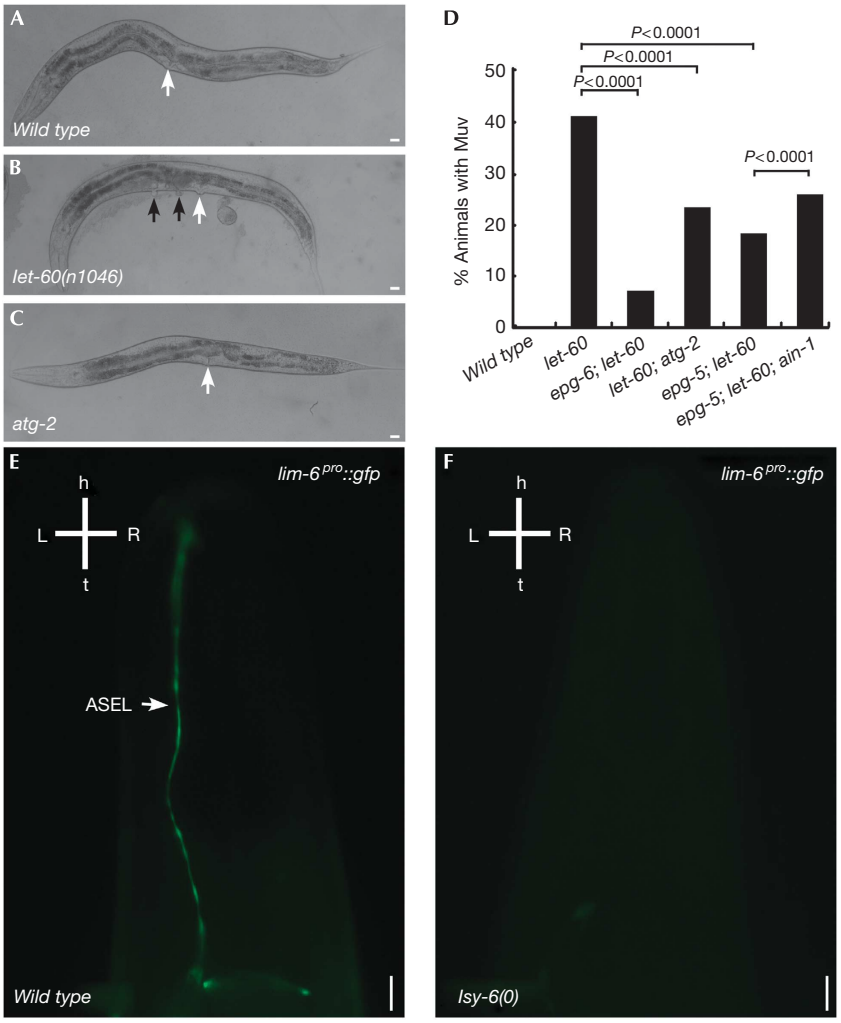

G

Animals expressing *lim-6^{pro} ::gfp* (%) in ASEL

	ASEL	ASER	ASEL	ASER	n	*P* value
Wild type	0		100		540	
atg-2	0		100		480	
epg-6	0		100		510	
lsy-6(ot150)	15.7		84.3		648	
lsy-6(ot150): atg-2	2.8		97.2		709	<0.0001[a]
atg-7; lay-6(ot150)	4.1		95.9		728	<0.0001[a]
epg-6; lsy-6(ot150)	6.9		93.1		807	<0.0001[a]
epg-5; lsy-6(ot150)	10.8		89.2		659	=0.009[a]
epg-1; lsy-6(ot150)	10.9		89.1		560	=0.01[a]
lsy-6(ot150); epg-7	8.9		91.1		727	<0.001[a]
sqst-1; lsy-6(ot150)	22.5		77.5		445	=0.33[a]
epg-2(RNAi); lsy-6(ot150)	15.0		85.0		427	=0.74[a]
let-363(RNAi); lsy-6(ot150)	28.5		71.5		411	<0.0001[a]
rheb-1 (RNAi); lsy-6(ot150)	21.2		78.8		458	<0.001[a]
lsy-6(ot150); ain-1(ku322)	41.7		58.3		525	<0.0001[a]
epg-5; lsy-6(ot150); ain-1(ku322)	35.9		64.1		476	<0.0001[b]
lsy-6(ot71)	100		0		440	
lsy-6(ot71); atg-2	100		0		432	

Fig 2 | Autophagy regulates developmental processes specified by the *let-7* miRNA family and *lsy-6* miRNA. (**A–C**) Wild-type and *atg-2* hermaphrodites have a single vulva (arrow). (**B**) *let-60(n1046gf)* mutants show a Muv phenotype. Black arrows indicate pseudovulvae. (**D**) Loss of autophagy activity suppresses the Muv phenotype in *let-60(n1046)* mutants. The number of adult animals examined was: wild type ($n = 450$), *let-60* ($n = 406$), *epg-6; let-60* ($n = 444$), *let-60; atg-2* ($n = 803$), *epg-5; let-60* ($n = 672$), *epg-5; let-60*; *ain-1(ku322)* ($n = 635$). *P* values are determined by a two-tailed χ^2 test. (**E,F**) *lsy-6* mutants show defects in ASEL fate specification and do not express the ASEL-specific reporter *lim-6^{pro}::GFP*. (**G**) Expression of *lim-6^{pro}::GFP* in various strains. [a]Compared with *lsy-6(ot150)*. [b]Compared with *lsy-6(ot150); ain-1(ku322)*. *P* values are determined by a two-tailed χ^2 test. (**A–C**) Scale bar, 20 μm; (**E,F**) scale bar, 10 μm. ASEL, ASE left; ASER, ASE right; GFP, green fluorescent protein; miRNA, microRNA; Muv, multivulva.

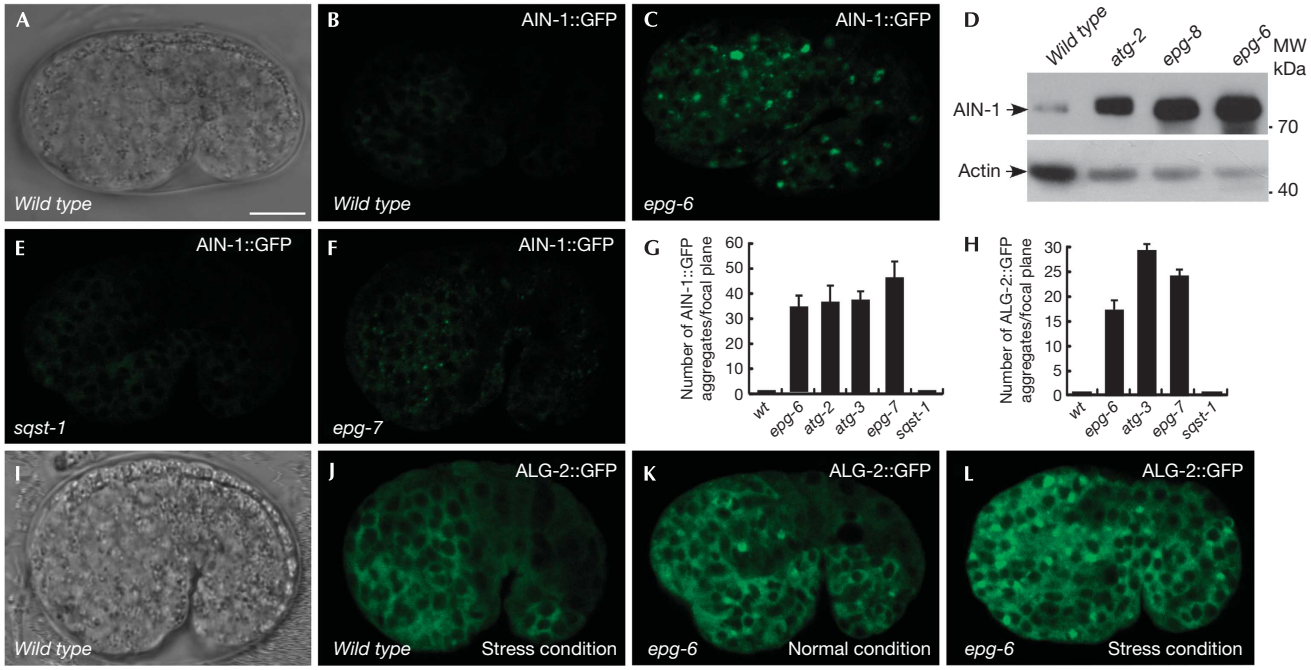

Fig 3 | AIN-1 is selectively degraded by autophagy. (**A,B**) AIN-1::GFP is weakly and diffusely expressed in the cytoplasm during embryogenesis in wild-type animals. (**A**) Nomarski image of the embryo shown in (**B**). Scale bar, 10 μm for whole embryo. *C. elegans* embryos remain the same size during embryogenesis and loss of autophagy activity has no effect on the embryo size. Thus, scale bars for embryos are only shown once in each figure. (**C**) AIN-1::GFP forms a large number of aggregates in *epg-6* mutant embryos. (**A–C**) are confocal images. (**D**) Western blotting shows that endogenous AIN-1 protein levels are dramatically elevated in autophagy mutant embryos compared with wild type. (**E**) No AIN-1::GFP aggregates are formed in *sqst-1* mutant embryos. (**F**) AIN-1::GFP accumulates into numerous aggregates in *epg-7* mutant embryos. (**G,H**) Number of AIN-1::GFP (**G**) and ALG-2::GFP (**H**) aggregates per focal plane in the indicated strains. Error bars indicate the s.d. of four examined embryos. (**I,J**) ALG-2::GFP is diffusely localized in the cytoplasm in wild-type embryos. (**I**) Nomarski image of the embryo shown in (**J**). (**K**) ALG-2::GFP forms a few aggregates in *epg-6* mutant embryos. (**L**) ALG-2::GFP forms a large number of aggregates in *epg-6* mutant embryos under stress conditions. GFP, green fluorescent protein; s.d., standard deviation.

number of aggregates dramatically increased under certain stress conditions (Figs 3H,K,L; supplementary Figs S2G,H,K,L online). ALG-1 levels also increased in autophagy mutants (supplementary Fig S2M online). *alg-1* and *alg-2* mRNA levels appeared normal in autophagy mutants (supplementary Figs S2N,O online). These results indicate that ALG-1 and ALG-2 accumulate into aggregates in autophagy mutants under certain stress conditions.

AIN-1 associates with SQST-1 aggregates

We next determined whether AIN-1 colocalizes with known protein aggregates in autophagy mutants. Maternally loaded germline P granule components PGL-1 and PGL-3 are degraded in somatic cells by autophagy during embryogenesis [26]. This process requires the self-oligomerizing receptor protein SEPA-1. In autophagy mutants, PGL-1/-3 and SEPA-1 accumulate into numerous aggregates, called PGL granules [26]. The *C. elegans* p62 homolog SQST-1 is also removed by autophagy and forms numerous aggregates in autophagy mutants [13]. PGL granules and SQST-1 aggregates are separable in various autophagy mutants, including mutants of the LGG-1/Atg8 conjugation system [13]. We found that in *atg-3* mutants, AIN-1::GFP aggregates largely colocalized with SQST-1 aggregates, but were separable from PGL granules (Figs 4A–L,Q). The EPG-6/ATG-2 complex is involved in progression of PI(3)P-enriched subdomains of the ER, called omegasomes, to autophagosomes [14]. *epg-6* and *atg-2* mutants show accumulation of LGG-1, the *C. elegans* Atg8 homolog, which associates with autophagosomal structures. In *epg-6* and *atg-2* mutants, LGG-1 puncta are enlarged and colocalize with SQST-1 aggregates [14]. Coimmunostaining showed that AIN-1 aggregates colocalized with LGG-1 puncta in *epg-6* mutants (Figs 4M–Q).

Colocalization of AIN-1 and SQST-1 aggregates in autophagy mutants prompted us to investigate the role of SQST-1/p62 in autophagic removal of AIN-1. Mammalian p62 acts as a receptor mediating the formation and autophagic degradation of ubiquitin-positive protein aggregates [16]. *C. elegans* SQST-1, as p62, self-interacts and directly associates with LGG-1/Atg8. In *sqst-1* mutants, AIN-1::GFP expression was unchanged and no aggregates were formed (Figs 3E,G). AIN-1::GFP still formed aggregates in *lgg-1(RNAi); sqst-1* animals (supplementary Fig 2P online). Thus, *sqst-1* is not required for the removal of AIN-1 and its formation of aggregates in autophagy mutants. SQST-1 aggregates contain several other unrelated self-oligomerized proteins that are removed by autophagy in a *sqst-1*-independent manner [27], suggesting that AIN-1 can be recruited into SQST-1 aggregates by other components. Selective degradation of autophagy substrates under physiological

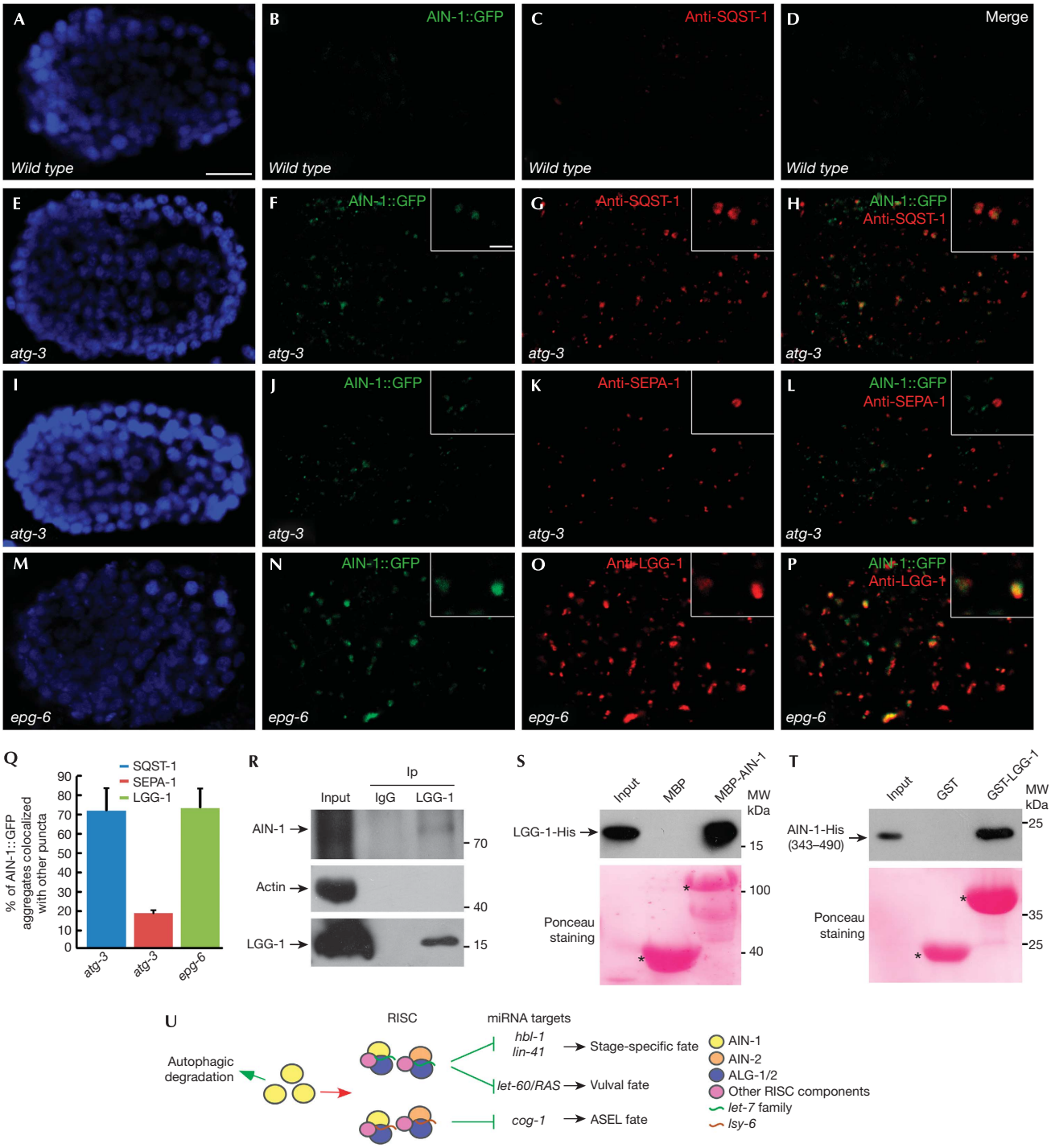

Fig 4 | AIN-1 colocalizes with SQST-1 aggregates in autophagy mutants and directly interacts with LGG-1. (**A–D**) Both AIN-1::GFP and SQST-1, detected by anti-SQST-1 antibody, are very weakly expressed and diffusely localized in wild-type embryos. (**E–H**) AIN-1::GFP aggregates colocalize with SQST-1 aggregates in *atg-3* mutant embryos. Scale bars, 10 μm for insets that show a magnified view. (**I–L**) AIN-1::GFP aggregates are separable from PGL granules, detected by anti-SEPA-1, in *atg-3* mutant embryos. (**M–P**) Colocalization of AIN-1::GFP aggregates with LGG-1 puncta in *epg-6* mutant embryos. (**Q**) % of AIN-1::GFP aggregates colocalized with SQST-1 aggregates, SEPA-1 aggregates and LGG-1 puncta in autophagy mutants. Error bars indicate the s.d. of four examined embryos. (**R**) A co-IP assay shows that AIN-1 associates with LGG-1 *in vivo*. (**S**) Direct interaction between AIN-1 and LGG-1 in an *in vitro* pull-down assay. 5% of the His fusion proteins used for pull-down are shown as input. Corresponding Ponceau-stained blots show the amount of proteins used for pull-down. (**T**) A fragment of AIN-1 directly binds to LGG-1 in an *in vitro* pull-down assay. (**U**) Model for the role of autophagy in modulating the miRNA pathway. co-IP, coimmunoprecipitation; GFP, green fluorescent protein; MBP, maltose-binding protein; miRNA, microRNA; IP, immunoprecipitant; RISC, RNA-induced silencing complex; s.d., standard deviation.

conditions requires a scaffold protein, which bridges the cargo/receptor complex to the autophagic machinery [27]. EPG-7 acts as a scaffold protein in mediating autophagic degradation of SQST-1 aggregates, but not PGL granule components [27]. EPG-7 itself is weakly expressed and diffusely localized in wild-type embryos and accumulates into numerous aggregates in autophagy mutants [27]. We found that loss of function of *epg-7* caused accumulation of AIN-1 aggregates (Figs 3F,G), indicating that EPG-7 mediates the autophagic degradation of AIN-1. GFP::ALG-1 and ALG-2::GFP aggregates also colocalized with SQST-1 aggregates but were separable from PGL granules in *atg-3* mutants (supplementary Figs S3A–Z online). GFP::ALG-1 and ALG-2::GFP accumulated in *epg-7* but not in *sqst-1* mutants (Fig 3H; supplementary Figs S3A2,B2 online). Consistent with the role of *epg-7* in degradation of AIN-1, the ASEL specification defect in *lsy-6(ot150)* mutants was suppressed by loss of activity of *epg-7*, but not *sqst-1* (Fig 2G). Loss of function of *epg-2*, which functions as a scaffold protein in mediating autophagic degradation of PGL granules but not SQST-1 aggregates [13], had no effect on the ASEL specification defect in *lsy-6(ot150)* mutants (Fig 2G).

AIN-1 directly interacts with LGG-1/Atg8

Direct interaction of substrates with Atg8/LC3 contributes to cargo specificity and degradation efficiency. Thus, we examined whether AIN-1 interacts with LGG-1. Using *in vivo* coimmunoprecipitation assays, we found that LGG-1 directly interacted with AIN-1, but not ALG-1 or ALG-2 (Fig 4R; supplementary Figs S4A–C online). His-fused LGG-1 interacted with maltose-binding protein-tagged AIN-1 *in vitro* (Fig 4S). His-fused AIN-1 also associated with GST-tagged LGG-1 and the LGG-1 binding region in AIN-1 was delineated to amino acids 343–490 (Fig 4T; supplementary Figs S4D–F online). This region contains two LIR motifs (Atg8/LC3-interacting region), ^{437}WGEL^{440} and ^{462}WNDL^{465}. Mutating either one or two LIR motifs did not alter LGG-1 binding, indicating that the LIR motif is not required for binding of AIN-1 to LGG-1 (supplementary Figs S4G–I online).

In conclusion, autophagy modulates diverse developmental processes specified by the miRNA pathway during *C. elegans* development. In mammalian cells, DICER and AGO2, but not GW182, are targeted for selective autophagic degradation [18]. Degradation of DICER and AGO2 is mediated by the selective autophagy receptor NDP52, which associates with the cargoes and also with Atg8/LC3 [18]. No obvious NDP52 homologs are found in *C. elegans*. The presence of distinct autophagy receptor and scaffold proteins might help determine whether different components of the RISC complex are degraded by autophagy in *C. elegans* and mammals. In contrast to *C. elegans*, the efficiency of miRNA-mediated silencing is reduced in autophagy-deficient mammalian cells [18]. The effect of autophagy on miRNA activity might depend on whether the degraded component acts before or after miRISC assembly. Our study reveals that autophagy modulates miRNA activity under physiological conditions.

METHODS

See supplementary information online for a list of strains, sequence for reporter construction and RNAi, antibody preparation and stress assay.

Indirect immunofluorescence. Permeabilization of embryos was performed by freeze-cracking methods. Freeze-cracked slides were fixed, blocked and incubated with diluted antibody at 4 °C overnight. Animals were then washed three times with phosphate-buffered saline with 2% Tween-20 (PBST) and incubated with fluorescently labeled secondary antibody at room temperature for 1 h. Slides were viewed using a confocal microscope (Zeiss LSM 510 Meta plus Zeiss Axiovert zoom, LSM Image Browser software). To compare the relative fluorescence intensity of gfp reporters, images were taken using the same exposure time and were measured using ImageJ software.

Supplementary information is available at *EMBO reports* online (http://www.emboreports.org).

ACKNOWLEDGEMENTS

We thank Dr Isabel Hanson for editing the manuscript. Some strains were provided by the *Caenorhabditis* Genetics Center (CGC). This work was supported by the National Basic Research Program of China (2013CB910100, 2011CB910100) and also a grant from the National Natural Science Foundation of China (31225018) to H.Z. The research of H.Z. was supported in part by an International Early Career Scientist grant from the Howard Hughes Medical Institute.

Author contributions: P.P.Z. and H.Z. designed the experiments, analysed the data and wrote the manuscript. P.P.Z. performed the experiments.

CONFLICT OF INTEREST

The authors declare that they have no conflict of interest.

REFERENCES

1. Carthew RW, Sontheimer EJ (2009) Origins and mechanisms of miRNAs and siRNAs. *Cell* **136:** 642–655
2. Ding L, Han M (2007) GW182 family proteins are crucial for microRNA-mediated gene silencing. *Trends Cell Biol* **17:** 411–416
3. Ambros V (2011) MicroRNAs and developmental timing. *Curr Opin Genet Dev* **21:** 511–517
4. Slack FJ, Basson M, Liu Z, Ambros V, Horvitz HR, Ruvkun G (2000) The *lin-41* RBCC gene acts in the *C. elegans* heterochronic pathway between the *let-7* regulatory RNA and the LIN-29 transcription factor. *Mol Cell* **5:** 659–669
5. Abbott AL, Alvarez-Saavedra E, Miska EA, Lau NC, Bartel DP, Horvitz HR, Ambros V (2005) The *let-7* MicroRNA family members *mir-48*, *mir-84* and *mir-241* function together to regulate developmental timing in *Caenorhabditis elegans*. *Dev Cell* **3:** 403–414
6. Li M, Jones-Rhoades MW, Lau NC, Bartel DP, Rougvie AE (2005) Regulatory mutations of *mir-48*, a *C. elegans let-7* family MicroRNA, cause developmental timing defects. *Dev Cell* **9:** 415–422
7. Johnson SM, Grosshans H, Shingara J, Byrom M, Jarvis R, Cheng A, Labourier E, Reinert KL, Brown D, Slack FJ (2005) RAS is regulated by the *let-7* microRNA family. *Cell* **120:** 635–647
8. Sternberg PW, Han M (1998) Genetics of RAS signaling in *C. elegans*. *Trends Genet* **14:** 466–472
9. Johnston RJ, Hobert O (2003) A microRNA controlling left/right neuronal asymmetry in *Caenorhabditis elegans*. *Nature* **426:** 845–849
10. Hammell CM, Lubin I, Boag PR, Blackwell TK, Ambros V (2009) *nhl-2* modulates microRNA activity in *Caenorhabditis elegans*. *Cell* **136:** 926–938
11. Ren HY, Zhang H (2010) Wnt signaling controls temporal identities of seam cells in *Caenorhabditis elegans*. *Dev Biol* **345:** 144–155
12. Nakatogawa H, Suzuki K, Kamada Y, Ohsumi Y (2009) Dynamics and diversity in autophagy mechanisms: lessons from yeast. *Nat Rev Mol Cell Biol* **10:** 931–937
13. Tian Y *et al* (2010) *C. elegans* screen identifies autophagy genes specific to multicellular organisms. *Cell* **141:** 1042–1055

14. Lu Q, Yang PG, Huang XX, Hu WQ, Guo B, Wu F, Lin L, Kovács AL, Yu L, Zhang H (2011) The WD40 repeat PtdIns(3)P-binding protein EPG-6 regulates progression of omegasomes to autophagosomes. *Dev Cell* **21:** 343–357
15. Zhao HY, Zhao GY, Wang XW, Xu LJ, Miao L, Feng D, Chen Q, Kovács AL, Fan DS, Zhang H (2013) Mice deficient in *Epg5* exhibit selective neuronal vulnerability to degeneration. *J Cell Biol* **200:** 731–741
16. Johansen T, Lamark T (2011) Selective autophagy mediated by autophagic adapter proteins. *Autophagy* **7:** 279–296
17. Derrien B, Baumberger N, Schepetilnikov M, Viotti C, De Cillia J, Ziegler-Graff V, Isono E, Schumacher K, Genschik P (2012) Degradation of the antiviral component ARGONAUTE1 by the autophagy pathway. *Proc Natl Acad Sci USA* **109:** 15942–15946
18. Gibbings D, Mostowy S, Jay F, Schwab Y, Cossart P, Voinnet O (2012) Selective autophagy degrades DICER and AGO2 and regulates miRNA activity. *Nat Cell Biol* **14:** 1314–1321
19. Grishok A, Pasquinelli AE, Conte D, Li N, Parrish S, Ha I, Baillie DL, Fire A, Ruvkun G, Mello CC (2001) Genes and mechanisms related to RNA interference regulate expression of the small temporal rnas that control *C. elegans* developmental timing. *Cell* **106:** 23–34
20. Ding L, Spencer A, Morita K, Han M (2005) The developmental timing regulator AIN-1 interacts with miRISCs and may target the argonaute protein ALG-1 to cytoplasmic P bodies in *C. elegans*. *Mol Cell* **19:** 437–447
21. Zhang L, Ding L, Cheung TH, Dong MQ, Chen J, Sewell AK, Liu X, Yates JR III, Han M (2007) Systematic identification of *C. elegans* miRISC proteins, miRNAs, and mRNA targets by their interactions with GW182 proteins AIN-1 and AIN-2. *Mol Cell* **28:** 598–613
22. Huang XX, Zhang H, Zhang H (2011) The zinc-finger protein SEA-2 regulates larval developmental timing and adult life span in *C. elegans*. *Development* **138:** 2059–2068
23. Lin SY, Johnson SM, Abraham M, Vella MC, Pasquinelli A, Gamberi C, Gottlieb E, Slack FJ (2003) The *C. elegans* hunchback homolog, *hbl-1*, controls temporal patterning and is a probable microRNA target. *Dev Cell* **4:** 639–650
24. Abrahante JE, Daul AL, Li M, Volk ML, Tennessen JM, Miller EA, Rougvie AE (2003) The *Caenorhabditis elegans* hunchback-like gene *lin-57/hbl-1* controls developmental time and is regulated by microRNAs. *Dev Cell* **4:** 625–637
25. Cai QC, Sun YY, Huang XX, Guo C, Zhang YX, Zhu ZY, Zhang H (2008) The *Caenorhabditis elegans PcG*-like gene *sop-2* regulates the temporal and sexual specificities of cell fates. *Genetics* **178:** 1445–1456
26. Zhang YX *et al* (2009) SEPA-1 mediates the specific recognition and degradation of p granule components by autophagy in *C. elegans*. *Cell* **136:** 308–321
27. Lin L, Yang PG, Huang XX, Zhang H, Lu Q, Zhang H (2013) The scaffold protein EPG-7 links cargo/receptor complexes with the autophagic assembly machinery. *J Cell Biol* **201:** 113–129